ROYAL SOCIETY OF CHEMISTRY

PAPER

Check for updates

Regulation of recombinant humanized collagen on HAP growth and its molecule simulation†

Zhilin Huang, [ID] ‡[ab] Chucheng Wang, [ID] ‡[ab] Xiaohui Chen,[ab] Shan Ding,[ab] Qi Xiang,[c] Mo Xie, [ID] [ad] Yadong Huang [ID] [c] and Hong Li [ID] ⋆[ab]

Hydroxyapatite (HAP) in natural bone is formed under the regulation of natural collagen I. Here, we report how recombinant humanized collagen I (rhCol I) regulates the growth of HAP nanocrystals in a long belt shape 100–150 nm in width and 200–300 nm in length. MD simulation results showed that the interactions between rhCol I and the (001), (100), and (211) planes of HAP mainly contributed to the electrostatic force and van der Waals forces via $COO\cdots Ca$, $-NH\cdots Ca$, $CH\cdots OPO_3$, and $NH\cdots OPO_3$ bonds, respectively. On the (001) plane, the interaction between $-COO^-$ and Ca was stronger than on the (100) and (211) planes, resulting in a large electrostatic force, which inhibited the growth of the (001) plane. The lowest energy of adsorption to the (211) plane resulted in the preferential growth of the (211) plane due to the weakest interaction with rhCol I. The detailed correlation between HAP and rhCol I could explain HAP growth under regulation by rhCol I. This study provides a reference for the bio-application of recombinant collagen.

1. Introduction

Hydroxyapatite (HAP, $Ca_{10}(PO_4)_6(OH)_2$)[1] is one of the most important components of bone minerals, and synthesized HAP shows great promise in hard tissue restoration.[2–5] Various synthesized HAP materials have been obtained and applied; however, these HAP materials, whose structure and biofunction are still far away from the natural bone apatite, still can not fully meet the requirements for the clinical treatment.[6,7] Therefore, the synthesis of HAP is still a hot topic in the biomedical field.

It is worth mentioning that bone is not monolithic but is essentially a nanohybrid, which constitutes HAP nanocrystals and collagen fibrils. HAP in natural bone is formed under the regulation of macromolecules via a process of biomineralization, in which collagen plays an important role.[8,9] As we know, collagen may initiate and direct the growth of apatite crystals, providing a structural template for the directed nucleation and growth of apatite.[10–12] Resembling bone formation in a biomimetic way, the HAP nanocrystals were prepared by regulating

the nucleation and growth of calcium phosphate minerals by collagen in an aqueous solution.[13] However, the use of natural collagen derived from animal tissue may raise many concerns related to the quality, purity, and possible immunological reactions,[14] and also can lead to a variability in cross-linking to the crystal phase, or changes in the nanostructure, or even the bio-functions of the formed HAP. Therefore, scientists are trying to find a biomolecule that possesses collagen's partial or full functions in the biomedical field, such as amino acids, peptides, and other proteins.[15]

With the progress in genetic engineering, recombinant collagen with designated structural and functional characteristics has been developed and shown potential in the biomedical field. Recombinant collagen is generally prepared by transcribing a specific gene segment and is expressed in yeast, bacteria, or animal cells,[16] with a consistent formulation output and high productivity. Considering the homology of the amino acid sequence, a human collagen gene that encodes a specific type of human collagen is mainly chosen to produce predictable and reliable recombinant collagen. In the early days, Cui *et al.* investigated the mineralization of recombinant human-like collagen, and found that it could regulate the deposition of HAP nanocrystals by the self-assembly of nano-fibrils of mineralized collagen.[17] However, there was some differences between the amino acid sequences of recombinant human-like collagen and native type I collagen, because some modification was done in the recombinant collagen due to solubility issues. More recently, in March 2021, a standard guide for the definition of recombinant collagen was issued by the National Medical Products Administration of China (NMPA), and

[a]College of Chemistry and Materials Science, Jinan University, Guangzhou, 510632, China. E-mail: tlihong@jnu.edu.cn

[b]Engineering Research Center of Artificial Organs and Materials, Ministry of Education, Guangzhou, 510632, China

[c]Institute of Biomedicine and Guangdong Provincial Key Laboratory of Bioengineering Medicine, Jinan University, Guangzhou, 510632, China

[d]Guangdong Provincial Key Laboratory of Functional Supramolecular Coordination Materials and Applications, Guangzhou, 510632, China

‡ These authors contributed equally to the work.

recombinant humanized collagen (rhCol I) was defined as a full-length or fragment of a functional amino acid sequence encoded by a specific type of human collagen gene, or a combination of the above functional fragments. RhCol I has the advantages of processability, being virus-free and water-soluble, and low immunogenicity, which we speculate mean it can be considered to regulate the formation of HAP in a biomimetic way.

In the study, we tried to explore the regulation of rhCol I on HAP growth. Although both collagen and noncollagenous proteins have been reported to contribute to the biomineralization of HAP,[18,19] the collagen-assisted mineralization mechanism at the molecular level is still underdeveloped. Xue *et al.*, using computational modeling, performed a detailed analysis of the Ca–P cluster growth process in the solution phase in the presence of human type I collagen, and revealed a nonclassical nucleation pathway for the HAP nucleation with the collagen I as the seed.[20] In recent studies, molecular dynamics (MD) simulations have been employed as an efficient method to understand the interactions between collagen and the HAP face.[21,22] The interaction sites,[23–25] adsorption energies,[26] substitution energies,[27,28] and other information were obtained based on MD simulations. Even, the interfacial interactions between the HAP crystallographic surfaces and complex polymers (such as PE, PLA, and PA66) have been studied by calculating their binding energies.[29] So far, and to the best of our knowledge, no study has yet analyzed the interaction between HAP and rhCol I. Herein, we employed MD simulation to study the interfacial interactions between HAP crystallographic surfaces and rhCol I. The study might help to explain the rhCol I dependence on HAP growth, and may provide support to develop novel biomaterials for tissue repair.

2. Experimental

2.1 Simulation and models

2.1.1 Models of the HAP crystal planes. The initial model of HAP ($P6_3/m$) was obtained from the crystal structure database,[30] with lattice parameters of $a = b = 9.421$ Å, $c = 6.880$ Å, $\alpha = 90°$, $\beta = 90°$, and $\gamma = 120°$. In HAP crystals, OH ions are arranged in parallel along the c-axis, while PO_4^{3-} groups exist as tetrahedra, with P^{5+} ions as the center and 4 oxygen atoms as the tips of the tetrahedron. Finally, the model was geometrically optimized to obtain a model structure with a global energy minimum. The final simulation consisted of one collagen molecule and 5000–6000 water molecules, the (001) crystal plane containing 3834 atoms, (100) crystal plane containing 3864 atoms, and (211) crystal plane containing 3808 atoms. The dimensions of the HAP surfaces used for the HAP-rhCol I interface simulations were $110 \times 41 \times 33$ Å for HAP (001), $110 \times 36 \times 37$ Å for HAP (100), and $115 \times 34 \times 36$ Å for HAP (211), respectively, as shown in Fig. 1.

2.1.2 Models of rhCol I. Water-soluble rhCol I was obtained from Jinan University (Guangzhou, China), which was prepared using *E. coli*. Since there is no crystal structure reported of the protein, we used trRosetta[31] to predict the 3D structures of the rhCol I (Fig. 2a). All the full-length sequences of 275 amino

acids (AAs) can be found in Fig. 2b, with 154 AA the same as those of human beings.

2.1.3 Simulation procedure. All simulations were performed with Materials Studio 2020 and using the Dreiding force field. The Dreiding force field is a generic force field and is designed for application to a wide range of systems (organic, biological, and main group inorganic molecules) containing a variety of different atoms.[32] It has been successfully applied in a large number of molecular dynamics simulations, including with HAP,[33,34] such as the study of the adsorption of zoledronic acid molecule on the hydroxyapatite (001) surface by Ri *et al.*[35] All the models were minimized by the conjugate gradient method prior to MD. Structural optimization of the rhCol I molecule was achieved with the Forcite[36] module. The HAP-rhCol I model was constructed by randomly placing collagen molecules on the HAP surface surrounded by water. All the simulation systems were set to an NVT ensemble with an integration timestep of 1 fs. The simulated temperature of the system was set to 298 K and a velocity scale thermostat was used for temperature coupling. Electrostatic interactions were calculated using the Ewald addition method and van der Waals interactions were calculated based on the atom based method, and their cut-off distance was 12.5 Å. The simulated annealing method was performed during 500 ps to gently carry the system from 273 to 313 K, simulating the experimental temperature conditions. After this procedure, one of the frames had the lowest energy, which was the most stable structure. Then, the structure was relaxed again by optimization. The dynamic trajectory for each system was finally recorded for statistical analysis at 1000 fs intervals during the next 1 ns of MD simulations.

The adsorption energies due to the interaction of the collagen and HAP surfaces were calculated according to eqn (1):[37]

$$E_{ads} = E_{gra} + E_{molecule} - E_{tot} \tag{1}$$

where E_{tot} is the energy of the optimized system; E_{gra} is the energy of the Ca–P; and $E_{molecule}$ is the energy of the collagen.

2.2 Synthesis of HAP crystals

Calcium chloride ($CaCl_2$, purity ≥ 96 wt%), and dipotassium hydrogen phosphate (K_2HPO_4, purity ≥ 99 wt%) were purchased from Sigma-Aldrich. All chemicals were used without further purification. The solutions were prepared with ultrapure water (0.22 lS, 25 °C, MilliQ©, Millipore).

First, 30 mM $CaCl_2$ solution and 3 mM K_2HPO_4 solution as the stock liquids were prepared, and then appropriate amounts of the $CaCl_2$ and K_2HPO_4 stock liquid were taken respectively and added into a centrifuge tube containing rhCol I solution. The final concentrations of $CaCl_2$, K_2HPO_4, and rhCol I were 2.5 mM, 1.5 mM, and 200 μg mL^{-1} respectively. Finally, the mixed solution was placed in a constant temperature water bath at 37 °C for mineralization for 3 days, and the precipitate was taken out after centrifugation and washed several times using
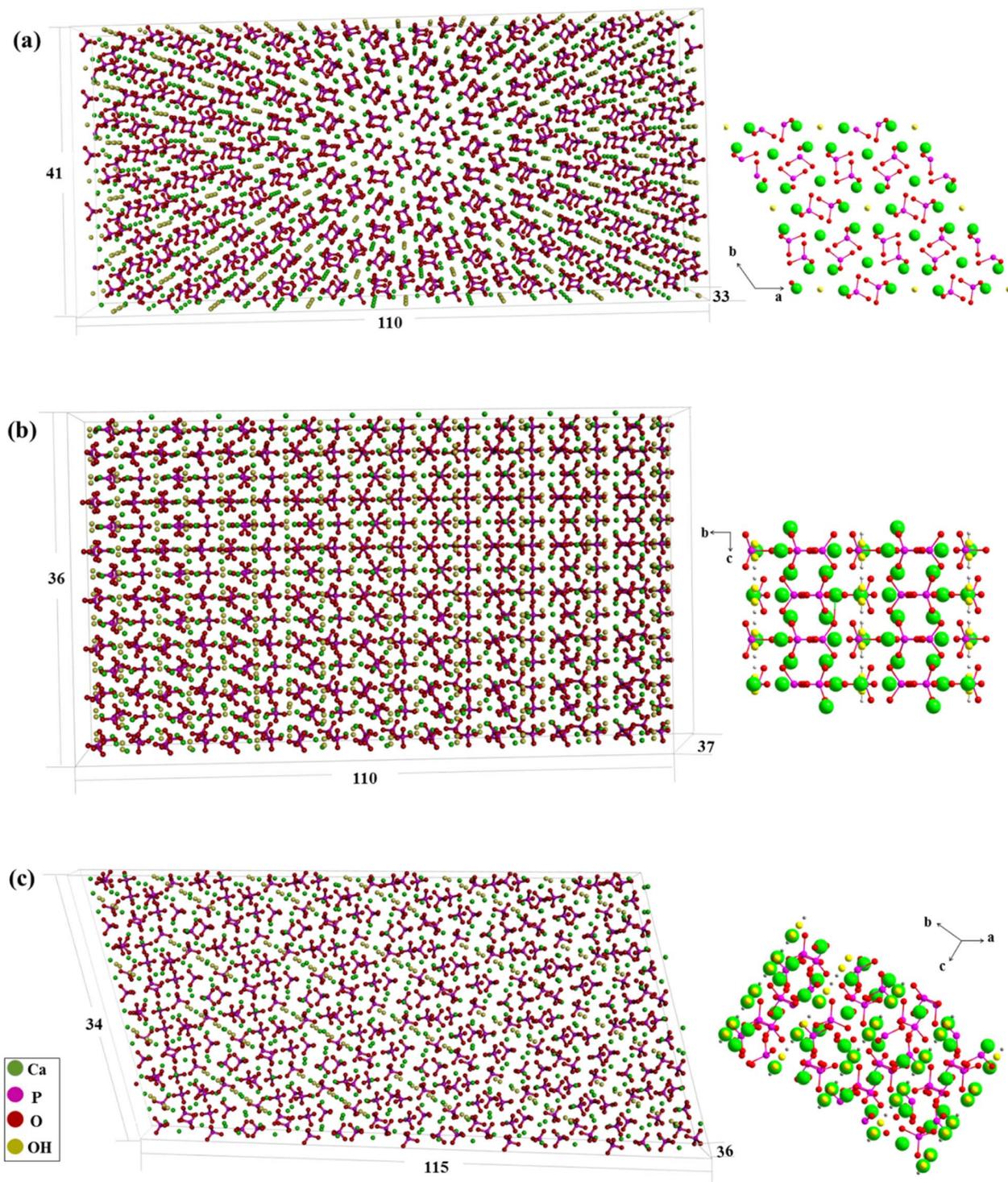
Fig. 1 Ball-and-stick models of HAP surfaces. (a) HAP (001); (b) HAP (100); (c) HAP (211).

ultrapure water. As a control, the above reaction was carried out in the absence of rhCol I.

2.3 Characterization

2.3.1 X-Ray diffraction (XRD). The samples were centrifuged after reaction, washed three times with ultrapure water,

and dried at room temperature prior to XRD analysis. The samples were analyzed over a 2-theta scan range from 5°–60° and compared with the established JCPDS card (09-0432) to match the peaks. The analysis was done using a MiniFlex600 instrument. The values of the cell parameters a and c can be calculated from formula (2) and the crystal size can be calculated from formula (3):

(a)

(b)

HHHHHHPAPTDLKFTQVTPTSLSAQWTPPNVQLTGYRVRVTPKEKTGPMFVAQCHPFSCARKFHGLM
VDCTCLVSVYALKDTLTSRPAQGVVTTLENVSPPRRARVTDATETTITISWRTKTETITGFQVDAVPANG
QTPIQRTIKPDVRSYTITGLQPGTDYTVGMQWLNDNARSSPVVIDASTAIDAPSNLRFLATTPNSLLRY
HQRTNTNVMPWFVPVTEGAEALTARVNLNLPGVTEATITGLEPGTEYTIYVIALKNNQKSEPLIGRKKT

Fig. 2 (a) Model of rhCol I. The colors represent the secondary structure of the collagen: blue represents sheet; green represents turn and gray represents coil. (b) Amino acid sequence of rhCol I.

$$\frac{1}{d^2} = \frac{4}{3}\left[\left(h^2 + hk + k^2/a^2\right)\right] + \frac{1}{c^2} \qquad (2)$$

$$D = k\lambda/(\beta\cos\theta) \qquad (3)$$

In formula (3), D is the crystal diameter, k is the ratio constant of 0.89, λ is the wavelength of the X-ray of 0.15406 nm, β is the width of the diffraction peak, and θ is the corresponding angle of the diffraction peak.

2.3.2 Transmission electron microscopy (TEM). Sample preparation for TEM was achieved by extracting an about 40 μL aliquot from the HAP-forming solution and then dropping this onto carbon film-supported copper grids (300 mesh, Ted Pella) and then leaving to air-dry overnight. The samples were then examined by TEM (JEM 2100F) to obtain bright-field and high-resolution images.

3. Results and discussion

3.1 Synthesized HAP

HAP crystals were observed *via* TEM as shown in Fig. 3a and b. It could be clearly seen that the synthesized HAP in the presence of the collagen had a belt-like structure, and these belts were 100–150 nm in width and 200–300 nm in length. However, it was found that plate-like HAP crystals 10–20 nm in width and 20–50 nm in length long formed in the control (Fig. 3b). In this case, we suppose that rhCol I acts as a soft template to guide and regulate HAP crystal growth with a long belt structure. The crystal structure of HAP in the presence of the rhCol I was further confirmed by selected area electron diffraction (SAED), as shown in Fig. 3c. The pattern of both HAP crystals showed a polycrystalline ring, and resolvable ring patterns ascribed to

the (002), (211), and (300) planes of the HAP, respectively. The crystal structure was further evaluated by HRTEM lattice fringes (Fig. 3d). The lattice fringes of the synthesized HAP in the presence of the rhCol I showed a *d*-spacing of 0.2817 nm, corresponding to (211) planes.

The XRD patterns shown in Fig. 3e gave all standard peaks matching with the JCPDS 09-0432 card of standard HAP, thus confirming the formation of the HAP phase in all the samples. The diffraction peak of the three main groups of HAP synthesized by rhCol I was at about 32°, corresponding to the (211), (112), and (300) crystal planes of HAP, and the peak shape was sharp and the intensity was high, indicating that the crystallinity of HAP was incisive. The diffraction peak intensity ratios of (211) to the (002) crystal plane in the standard HAP (JCPDS 09-0432) and blank control groups were 2.5 and 1.69, respectively, while the diffraction peak intensity ratio of the existing (211) to (002) crystal plane in the presence of rhCol I was 38.5, indicating that rhCol I made HAP grow preferentially along the (211) plane. The values for the HAP cell parameters and crystal size can be calculated by formulas (2) and (3), as shown in Table 1. The results show that the rhCol I regulated the crystal growth of HAP, which caused the cell parameters to increase the *a* value and decrease the *c* value. The crystal size increased to 50.300 nm according to Table 1.

Most studies suggest that the interaction between the collagen matrix and HAP crystals determines the eventual morphology of the HAP platelets in the bone.[38,39] The (001) crystal plane is the most stable of all the crystal planes of HAP, and the interaction on the (001) crystal plane determines the morphology of HAP in the presence of proteins.[40] However, HAP crystals in tooth enamel with high crystallinity have shown that matrix proteins only affect the growth of the (010) surface.[41] This
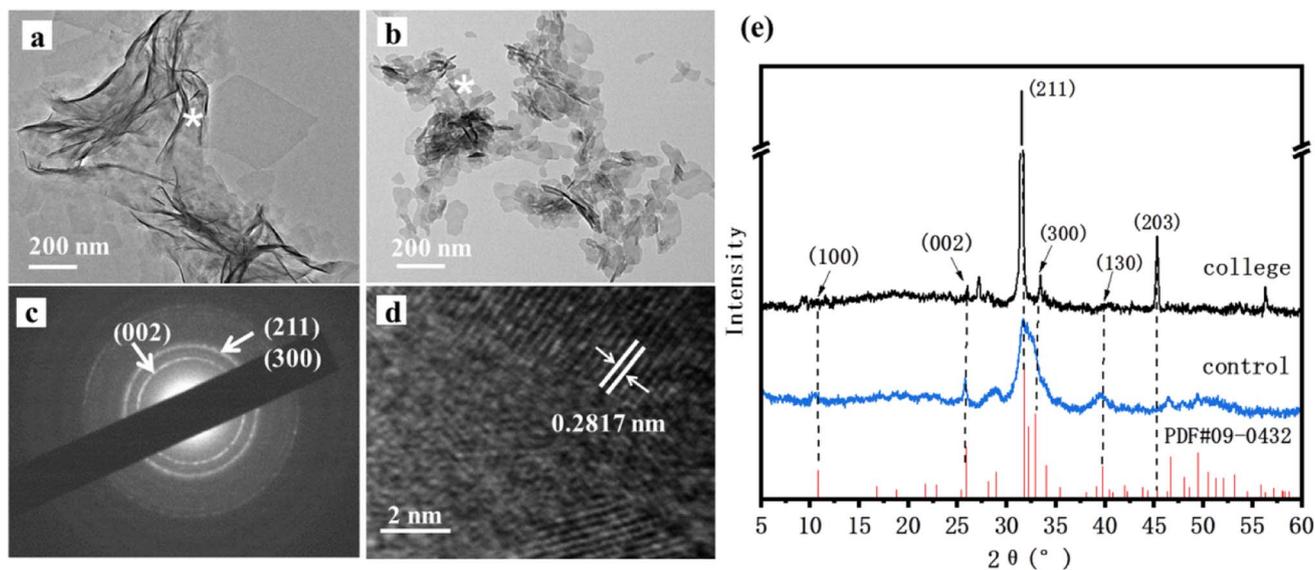
Fig. 3 (a) TEM images showing HAP samples synthesized in collagen; (b) TEM images of the control group; (c) SADE images; (d) HRTEM images; (e) XRD patterns. Asterisks indicate the corresponding SADE mode in the region.

Table 1 Cell parameters and sizes of HAP generated in the presence of rhCol I

Sample	a (Å)	c (Å)	c/a	D (Å)
HAP (JCPDS 09-0432)	9.418	6.884	0.731	—
Blank control group	9.473	6.852	0.723	216.200
rhCol I	9.523	6.820	0.716	503.000

means that the interaction between the matrix and HAP also affects its preferential growth at different planes. Also, although most of the prior studies have shown the strong growth of (211) plane as the HAP crystal,[42] no details about the interaction of HAP on the (211) plane have been reported. Herein, we tried to analyze the interaction between rhCol I and the (001) plane, (100) plane, and (211) plane using MD simulations.

3.2 Interaction between HAP and rhCol I

Generally, there are multiple steps for the interaction of biomolecules on the HAP surface: first of all, the molecule would spread to the HAP surface and then be adsorbed at the active site of the HAP surface, eventually overlapping the structure after adsorption. As studied by Xue[11] and Almora-Barrios,[13] type I collagen can maintain a stable structure quite well, so we assumed that the rhCol I can keep the same configuration, as shown in Fig. 2a. Detailed information on the active sites of rhCol I for the (001), (100), and (211) surfaces of HAP was obtained and is shown in Fig. 4–6 and Fig S1–S6,† respectively.

Looking at 3 parts of rhCol I, Part 1 was adsorbed at the (001) surface, as shown in Fig. 4a, and Part 2 and Part 3 on the (001) crystal plane, as shown in Fig. S1 and S2,† respectively. The most common interaction site of full-length rhCol I on the HAP (001) surface is between the hydrogen atom of $-CH_2$ groups with

the oxygen atom of the phosphoric acid group ($CH\cdots OPO_3 = 1.686$–3.967 Å), and the average interaction distance was 2.703 Å, according to our analysis as shown in Fig. 4b. Also, the oxygen atom of the carboxylic acids and the hydrogen atom of the $-CH_2$ group can interact strongly with surface calcium ions ($COO\cdots Ca = 1.496$–3.513 Å, $-CH\cdots Ca = 1.471$–3.910 Å), respectively. It has been reported that the hydrogen atoms of the amine group ($>NH_2$) will migrate to the oxygen atoms of the phosphoric acid group on the surface, which will form hydrogen bonds,[21] whose range for $NH\cdots OPO_3$ is 2.072–3.701 Å. In addition, the hydrogen atom of the amine group has a small amount of interaction with surface calcium ions ($-NH\cdots Ca = 2.007$–3.655 Å).

As shown in Fig. 5a, S3 and S4,† the rhCol I molecule was adsorbed on the (100) surface of HAP. The shortest average adsorption distance was between the hydrogen atoms of $-CH_2$ groups with the oxygens of hydroxide ($CH\cdots OH$), and the average adsorption distance was 2.702 Å. The most favorable mode of adsorption for the rhCol I is through a lot of interactions between the hydrogen atoms of $-CH_2$ groups with the oxygen atom of the phosphoric acid group ($CH\cdots OPO_3 = 2.314$–3.740 Å), because they have the largest number of interactions, and the adsorption distance was shorter with an average adsorption distance of 3.005 Å. Hydrogen bondings occur between the hydrogen atom of the amine group with the oxygen of the phosphoric acid group and the oxygens of hydroxide ($NH\cdots OPO_3 = 1.096$–3.842 Å, $NH\cdots OH = 3.089$–3.320 Å), which are in accord with results in the recent computational study of Almora-Barrios *et al.*[21,43] The hydrogen atoms of the amine group and the hydrogen atoms of the $-CH_2$ group also have a small amount of interaction with the surface calcium ions ($-NH\cdots Ca = 2.147$–3.501 Å, $-CH\cdots Ca = 1.747$–3.879 Å). The interaction of the oxygen atoms of the carboxyl group with surface calcium ion ($COO\cdots Ca = 3.123$ Å) was weaker than that on the (001) plane. However, the interaction between the oxygen
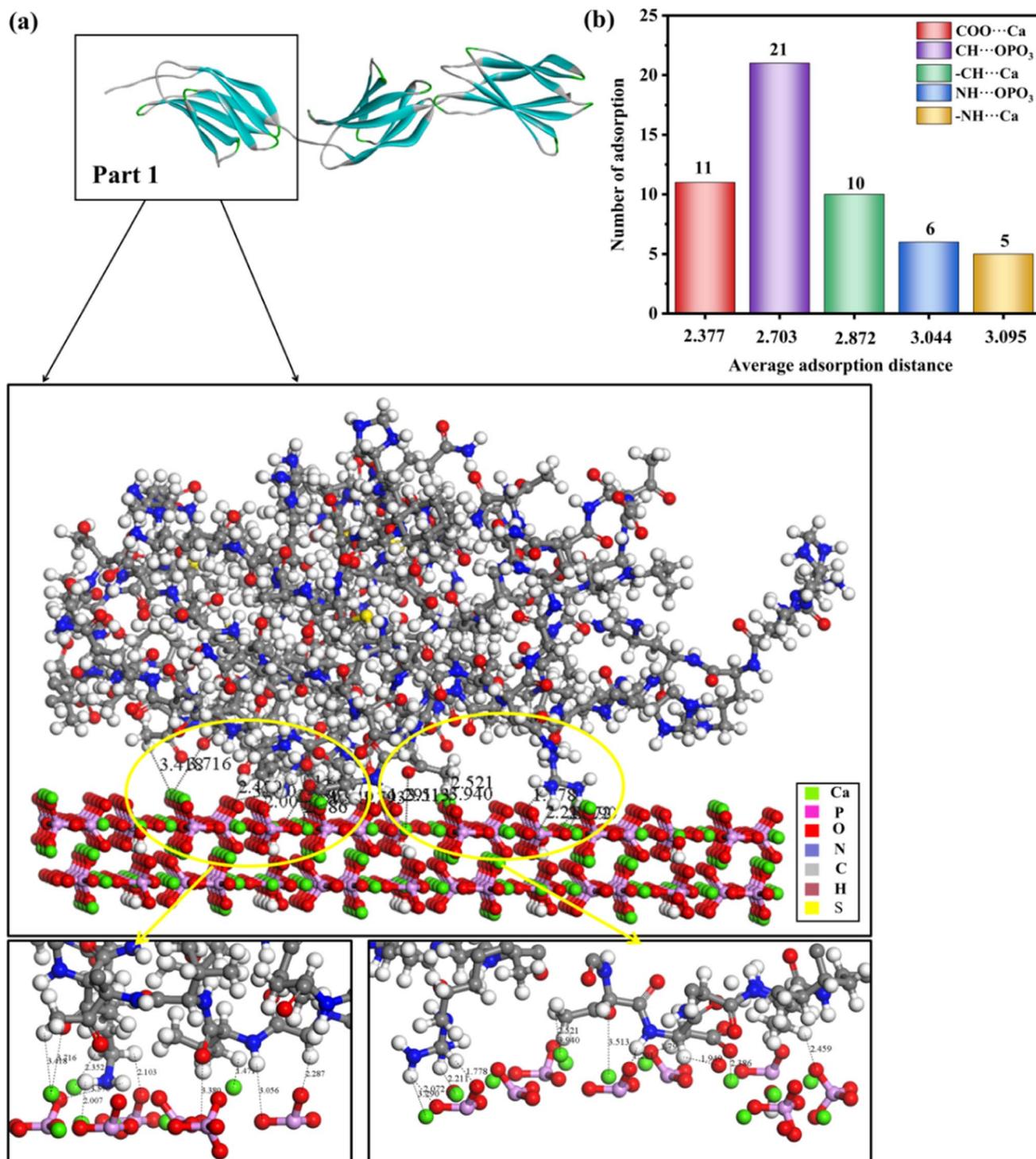
Fig. 4 (a) Adsorption configurations of rhCol I (Part 1) on the (001) surface and its local enlargement. In order to clearly observe the interaction between protein and HAP, no water molecules are shown. (b) Column diagram of the adsorption mode, the number of adsorption sites, and average adsorption distance of full-length rhCol I on the (001) plane of HAP. The horizontal coordinate of the column diagram represents the average adsorption distance, and the vertical coordinate represents the number of adsorption sites in the adsorption mode. The distance unit is Å.

atom of the carboxyl group and the hydrogen atom of the hydroxyl group (COO···HO = 2.560–3.967 Å) was stronger than that of the (001) plane.

Fig. 6, S5 and S6† show the lowest-energy configuration on the (211) surface, where the shortest average adsorption distance was between the hydrogen atoms of the amine group with the calcium ions on the surface (−NH···Ca = 2.201–3.352
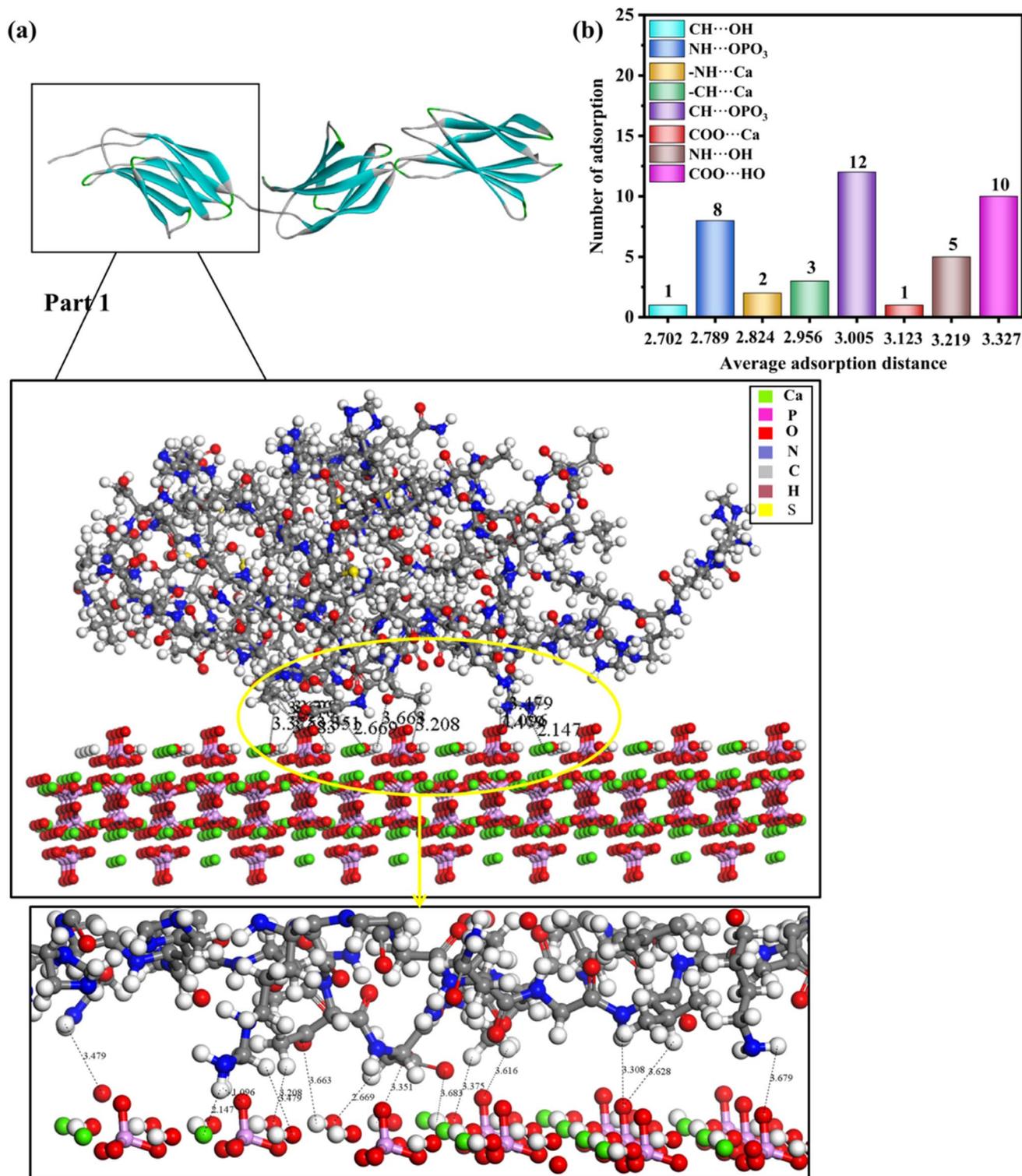
Fig. 5 (a) Adsorption configurations of rhCol I (Part 1) on the (100) surface and its local enlargement. In order to clearly observe the interaction between protein and HAP, no water molecules are shown. (b) Column diagram of the adsorption mode, the number of adsorption sites, and average adsorption distance of full-length rhCol I on the (100) crystal plane of HAP. The horizontal coordinate of the column diagram represents the average adsorption distance, and the vertical coordinate represents the adsorption frequency in the adsorption mode. The distance unit is Å.

Å), and the average adsorption distance was 2.954 Å. In addition, the interaction with the surface occurs mainly *via* the hydrogen atom of the –CH$_2$ group and the hydrogen atoms of

the amine group with the oxygen of the phosphoric acid group (CH···OPO$_3$ = 2.240–3.889 Å, NH···OPO$_3$ = 2.326–3.951 Å). The oxygen atoms of the carboxyl group and the hydrogen atoms of
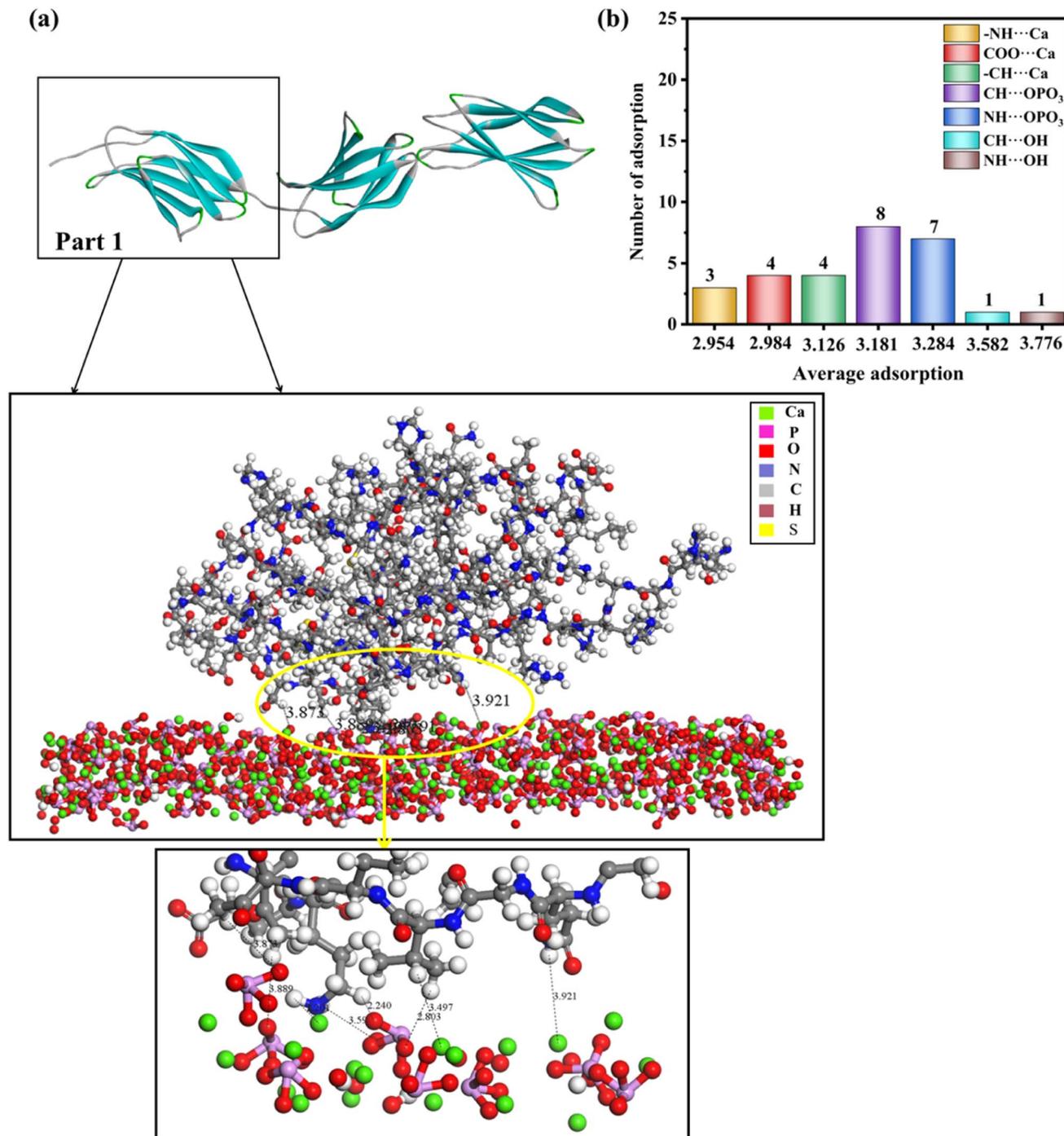
Fig. 6 (a) Adsorption configurations of rhCol I (Part 1) on the (211) surface and its local enlargement. In order to clearly observe the interaction between protein and HAP, no water molecules are shown. (b) Column diagram of the adsorption mode, the number of adsorption sites, and average adsorption distance of full-length rhCol I on the (211) plane of HAP. The horizontal coordinate of the column diagram represents the average adsorption distance, and the vertical coordinate represents the adsorption frequency in the adsorption mode. The distance unit is Å.

the $-CH_2$ group will have relatively strong interactions with the calcium ions on the surface ($COO\cdots Ca = 2.798–3.118$ Å, $-CH\cdots Ca = 2.364–3.497$ Å), and the average adsorption distances were 2.954, 2.984, and 3.126 Å, respectively. In addition, the hydroxyl group on the (211) surface interacted only slightly with hydrogen atoms of the amine group and hydrogen atoms

of the $-CH_2$ group, because the number of interactions between them was minimal and the adsorption distance was longer.

Based on the analysis above, the interaction between rhCol I and HAP depends mainly on electrostatic interaction energy and van der Waals forces. As shown in Fig. 4–6, the interactions

between the rhCol I and (001), (100), and (211) planes of HAP were mainly via COO···Ca, –NH···Ca, CH···OPO₃, and NH··· OPO₃, respectively. These interactions mean that the growth of HAP also was affected by the main chain group of CH_2, which showed a crystal with a long belt shape. Relatively, the adsorption sites on the (001) plane were the most abundant (the total number of adsorption sites was 53), which means a strong interaction between the rhCol I and on the plane of HAP; meanwhile, the least was related to the adsorption sites on the (211) plane, which indicated a weak interaction between them.

Typically, almost all collagen peptides form multiple interactions with the HAP surface through –COO⁻ and >NH₂ groups,[44,45] and the electrostatic interaction is the main driving force of collagen, peptides, amino acids, and other proteins, where their functional groups, such as carboxylic acids, can directly bond with surface Ca ions.[46–48] For natural collagen, representing a triple-helical molecule consisting of two α1 chains and one α2 chain formed via chemical bonding and hydrogen bonding, free charged resides would be reserved. MD simulations indicated that these charged residues could allow the formation of CaP clusters.[20] Combined with previous reports,[49–51] it is argued that rhCol I has a stable molecular configuration, which may be formed via the interaction of electrostatic interaction; therefore, the electrostatic interaction and van der Waals forces are the main interactions between rhCol I and HAP crystals.

3.3 Absorption energy

A negative adsorption energy indicates that adsorption of a protein at the surface is thermodynamically favorable. Usually, if the adsorption distance on this surface is shorter, the interaction force will be stronger, leading to stronger adsorption on this surface, and then the adsorption energy will be higher. Based on the results of the MD simulations, we speculated that the adsorption energy of the (001) plane would be the highest and that of the (211) plane would be the weakest.
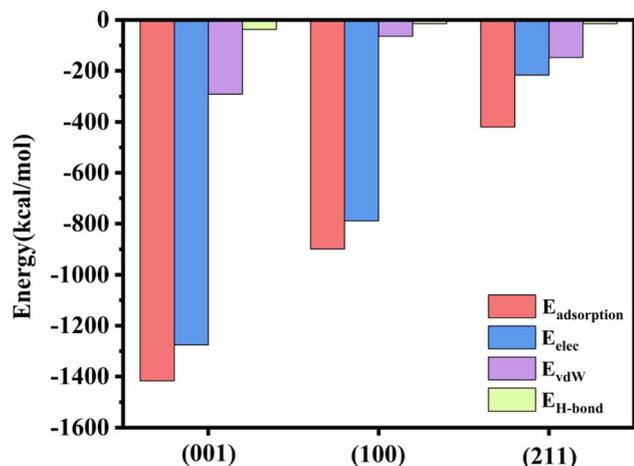
The adsorption energy is a macroscopic representation of the interaction force between molecules. The adsorption energy of the rhCol I on the surface of HAP was calculated according to eqn (1), as shown in Fig. 7. The electrostatic interaction energy plays an important role in the adsorption process here because the electrostatic interaction energy (E_{elec}) was significantly greater than the van der Waals interaction energy (E_{vdW}) and hydrogen bonding energy (E_{H-bond}). The adsorption energy of the rhCol I on the (001) crystal plane of HAP was the highest (-1417.262 kcal mol⁻¹); thus the adsorption was the strongest, indicating that rhCol I tends to be strongly adsorbed on the (001) surface. Then the inhibitory effect on the growth of the (001) surface had the strongest effect. However, the adsorption energy on the (211) plane was -419.841 kcal mol⁻¹, and the adsorption energy was the lowest. Therefore, it can be inferred that the growth of the (211) plane was greater than the other two planes, resulting in the obvious preferential growth of (211), which is consistent with the results from the experimental and MD simulation studies.

Besides, ongoing work in our group will take into account the effect of water and carbonate on the adsorption of collagen at HAP surfaces, which clearly takes place in an aqueous environment. The presence and competition of surrounding water molecules and carbonate may well affect the adsorption of the collagen to the HAP surfaces and hence HAP growth.

4. Conclusions

Based on MD simulation, the (001), (100), and (211) planes of HAP crystal strongly interact with rhCol I mainly via COO···Ca, –NH···Ca, CH···OPO₃, and NH···OPO₃, respectively, which can be related to the electrostatic interaction and van der Waals forces. On the (001) plane, the interaction between –COO⁻ and Ca was stronger than the other two crystal planes, resulting in a greater electrostatic force, which may result in a strong adsorption on the (001) plane, and further inhibit the growth of (001) of HAP. The free energy of adsorption of the rhCol I on the (001), (100), and (211) planes of HAP was in accord with the results from the MD simulation, respectively. Due to the lowest adsorption energy of (211) plane, preferential growth of the (211) plane was determined, which agreed with our experimental results. Here, MD simulations of rhCol I regulation of HAP crystal growth are presented, which may be helpful to synthesize HAP under regulation by novel biomolecules.

Author contributions

Zhilin Huang: methodology, date curation, writing-original draft. Chucheng Wang: methodology, date curation, investigation. Xiaohui Chen: investigation, validation. Hong Li: methodology, resources, writing-review & editing, funding acquisition. Shan Ding, Qi Xiang, Mo Xie, Yadong Huang: methodology, resources.

Conflicts of interest

There are no conflicts to declare.

Fig. 7 Value of adsorption energy, electrostatic energy, van der Waals energy, and hydrogen bonding energy of rhCol I on the crystal surface.

Acknowledgements

References

1 S. Awasthi, S. K. Pandey and E. Arunan, *J. Mater. Chem. B*, 2021, **9**, 228–249.

2 Z. Zou, J. Xie and E. Macías-Sánchez, *Cryst. Growth Des.*, 2020, **21**, 414–423.

3 T. W. Sun, Y. J. Zhu and F. Chen, *RSC Adv.*, 2018, **8**, 26218–26229.

4 X. Zheng, P. Zhang and Z. Fu, *RSC Adv.*, 2021, **11**, 19041–19058.

5 D. Luo, S. Lin and X. Li, *Mater. Lett.*, 2011, **65**, 2395–2397.

6 A. Hertz and I. J. Bruce, *Nanomedicine*, 2007, **2**, 899–918.

7 Y. Khan, M. J. Yaszemski and A. G. Mikos, *J. Bone Jt. Surg.*, 2008, **90**, 36–42.

8 F. Nudelman, K. Pieterse and A. George, *Nat. Mater.*, 2010, **9**, 1004–1009.

9 A.-W. Xu, Y. Maa and H. Cölfen, *J. Mater. Chem.*, 2007, **17**, 415–444.

10 Y. Wang, T. Azaïs and M. Robin, *Nat. Mater.*, 2012, **11**, 724–733.

11 Z. Xue, X. Wang and D. Xu, *Phys. Chem. Chem. Phys.*, 2022, **24**, 11370–11381.

12 L. Chen, R. Jacquet and E. Lowder, *Bone*, 2015, **71**, 7–16.

13 N. Almora-Barrios and N. H. De Leeuw, *Cryst. Growth Des.*, 2012, **12**, 756–763.

14 T. Luo and K. L. Kiick, *Eur. Polym. J.*, 2013, **49**, 2998–3009.

15 W. J. Chung, K. Y. Kwon and J. Song, *Langmuir*, 2011, **27**, 7620–7628.

16 T. Wang, J. Lew and J. Premkumar, *Eng. Biol.*, 2017, **1**, 18–23.

17 Y. Zhai, F. Z. Cui and Y. Wang, *Curr. Appl. Phys.*, 2005, **5**, 429–432.

18 A. L. Boskey, *Bone Miner.*, 1989, **6**, 111–123.

19 B. M. Oosterlaken, M. P. Vena and G. With, *Adv. Mater.*, 2021, **33**, 2004418.

20 Z. Xue, M. Yang and D. Xu, *J. Phys. Chem. C*, 2019, **123**, 2533–2543.

21 C. Liao, Y. Xie and J. Zhou, *RSC Adv.*, 2014, **4**, 15759–15769.

22 N. Almora-Barrios and N. H. de Leeuw, *Langmuir*, 2010, **26**, 14535–14542.

23 J. Zeng, S. Yang and H. Yu, *Langmuir*, 2021, **37**, 3410–3419.

24 J. W. Shen, T. Wu and Q. Wang, *Biomaterials*, 2008, **29**, 513–532.

25 S. Shang, Q. Zhao and D. Zhang, *Mater. Sci. Eng., C*, 2019, **105**, 110017.

26 S. E. Hoff, J. Liu and H. Heinz, *J. Colloid Interface Sci.*, 2022, **605**, 685–700.

27 X. Wang, L. Zhang and Z. Liu, *RSC Adv.*, 2018, **8**, 3716–3722.

28 X. Wang, X. Yang and H. Chen, *Langmuir*, 2020, **36**, 10822–10829.

29 H. Zhang, X. Lu and Y. Leng, *Acta Biomater.*, 2009, **5**, 1169–1181.

30 L. Veselinović, L. Karanović and Z. Stojanović, *J. Appl. Crystallogr.*, 2010, **43**, 320–327.

31 Z. Du, H. Su and W. Wang, *Nat. Protoc.*, 2021, **16**, 5634–5651.

32 S. L. Mayo, B. D. Olafson and W. A. Goddard, *J. Phys. Chem.*, 1990, **94**, 8897–8909.

33 M. S. Oliveira, S. N. Costa and N. K. V. Monteiro, *J. Braz. Chem. Soc.*, 2019, **30**, 2367–2375.

34 W. G. Knupp, M. S. Ribeiro and M. Mir, *Appl. Surf. Sci.*, 2019, **495**, 143493.

35 M. H. Ri, C. J. Yu and Y. M. Jang, *J. Mater. Sci.*, 2016, **51**, 3125–3135.

36 R. Gholizadeh and Y. Wang, *Chem. Eng. Sci.*, 2018, **184**, 62–71.

37 R. Bhowmik, K. S. Katti and D. Katti, *Polymers*, 2007, **48**, 664–674.

38 Y. F. Xu, F. Nudelman and E. D. Eren, *Nat. Commun.*, 2020, **11**, 1–12.

39 W. B. Tien, M. T. Chen and P. C. Yao, *Mater. Sci. Eng., C*, 2012, **32**, 2096–2102.

40 J. W. Shen, T. Wu and Q. Wang, *Biomaterials*, 2008, **29**, 513–532.

41 E. F. Bres and J. L. Hutchison, *J. Biomed. Mater. Res.*, 2002, **63**, 433–440.

42 Y. Zhai and F. Z. Cui, *J. Cryst. Growth*, 2006, **291**, 202–206.

43 N. Almora-Barrios, K. F. Austen and N. H. de Leeuw, *Langmuir*, 2009, **25**, 5018–5025.

44 H. Gu, Z. Xue and M. Wang, *J. Phys. Chem. B*, 2019, **123**, 3372–3382.

45 K. Wang, M. H. Wang and Q. G. Wang, *J. Eur. Ceram. Soc.*, 2017, **37**, 2509–2520.

46 M. Cutini, M. Corno and D. Costa, *J. Phys. Chem. C*, 2017, **123**, 7540–7550.

47 W. Wang, Z. Xue and D. Xu, *J. Phys. Chem. B*, 2021, **125**, 5078–5088.

48 Z. Wang, Z. Xu and W. Zhao, *J. Mater. Chem. B*, 2015, **3**, 9157–9167.

49 E. Troy, M. A. Tilbury and A. M. Power, *Polymers*, 2021, **13**, 3321.

50 P. V. Azzopardi, J. O'Young and G. Lajoie, *PLoS One*, 2010, **5**, e9330.

51 Y. Xie, C. Liao and J. Zhou, *Biophys. Chem.*, 2013, **179**, 26–34.